X-ray-standing-wave—modulated electron emission near absorption edges in centrosymmetric and noncentrosymmetric crystals

M. J. Bedzyk and G. Materlik
Hamburger Synchrotronstrahlungslabor (HASYLAB), Deutsches Elektronen-Synchrotron (DESY), D-2000 Hamburg 52, West Germany

M. V. Kovalchuk
Institute of Crystallography, Academy of Sciences of the Union of Soviet Socialist Republics, Moscow 117333, Union of Soviet Socialist Republics

(Received 31 October 1983; revised manuscript received 21 February 1984)

Energy-dispersive electron-emission yields were measured for (111) Bragg reflections of x rays from Ge and GaAs crystals. The reflection angle was changed continuously over the Bragg reflection range, thus causing the internal x-ray-standing-wave pattern to move across the atomic planes. With the use of synchrotron radiation, these measurements were performed at photon energies below and above the Ga and As K absorption edges. This introduces an energy-dependent position shift of the noncentrosymmetric diffraction planes relative to the atomic planes. It is shown how to determine, from such measurements, (i) the dispersion parameters f' and f''; (ii) lattice deviations, including amorphous and crystalline surface layers; (iii) a mean electron escape depth; and (iv) crystal polarity.

I. INTRODUCTION

The interpretation of dynamical x-ray diffraction in perfect crystals in terms of x-ray standing waves is well established since the discovery of the Borrmann effect.[1] This picture, which relates the x-ray-standing-wave field structure to the crystal structure, was at first applied to explain the anomalous transmission of incident x rays. Batterman[2] was the first to study a related emission process, namely the case of K fluorescence from a Ge crystal while Bragg reflecting incident Mo $K\alpha$ radiation. Other basic processes involved in x-ray scattering such as thermal diffuse scattering,[3,4] Compton scattering,[3,5,6] and electron emission[7,8] were also investigated.

In 1974, Golovchenko, Batterman, and Brown[9] used x-ray standing waves in combination with characteristic fluorescence radiation to determine the position of impurity atoms in a host lattice. Later, this technique was also applied to locate chemisorbed atomic layers on crystal surfaces.[10,11] Independently developed was a method to use electron emission for studying distortion profiles of disturbed surface layers[7] and of epitaxially grown surface layers with varying thicknesses.[12]

Previous to our investigation, x-ray-standing-wave measurements on noncentrosymmetric crystals have been used to determine the polarity of GaP crystals orientated in the (111) direction. Trucano[13] monitored the phosphorus K fluorescence as the nodal planes of the standing-wave field moved across the phosphorus atomic planes when sweeping through the (111) Bragg reflection and across the Ga atomic planes for the $(\overline{1}\overline{1}\overline{1})$ case. Subsequently, Takahashi and Kikuta,[8] performing a similar investigation, monitored the zero energy loss Ga L photoelectrons, using a cylindrical energy analyzer in a high-vacuum chamber.

Unlike the absorption length of the fluorescence radiation, the photoelectron escape depth is small in comparison to the extinction length of the incident x rays. This feature plus the depth-dependent electron energy-loss process give the photoelectron standing-wave measurement certain advantages in comparison to the fluorescence measurement. Since high-energy resolution photoelectron measurements need high-vacuum and longer data collection time, it can be advantageous to use a low-resolution electron counter.

Parallel to our investigation, Patel and Golovchenko,[14] in a standing-wave measurement on GaAs(111), have collected the fluorescence with a glancing angle detector geometry. Thus they reduced the extinction dip feature which masks structural information when the absorption length of the emitted radiation becomes comparable with the extinction depth of the incident radiation.

In this paper we report measurements made with noncentrosymmetric GaAs crystals along with comparative results from centrosymmetric Ge crystals, and show how a proportional counter can be used as an electron spectrometer in combination with synchrotron radiation. The energy tunability of the incident photons makes it possible to take measurements below and above the absorption edges of the atomic species which constitute the crystal. Thus, the experiment demonstrates how to measure the shift of the noncentrosymmetric diffraction planes with respect to the atomic lattice as a function of photon energy. This position shift is based on the fact that x-ray diffraction is connected with the Fourier component of the elastically scattered charge density described by the structure factor of the reflection which changes strongly close to absorption edges. The dispersion parameters f' and f'' are used to characterize the energy dependence of this process. Therefore, these can also be determined from

such measurements.

At a fixed incident photon energy, one can obtain structural information on different levels of spatial sensitivity by monitoring the electron emission at different angular points in the vicinity of the strong Bragg reflection. Electrons, which are inelastically scattered on their way out of the crystal, have a specific energy loss which is related to the depth at which the initial photon absorption and electron emission took place. This leads to structural information in units of the electron mean-free path. Atomic positions on the scale of the diffraction plane spacing can be determined by measuring the angular variation of the electron emission from a particular atomic species.

II. THEORY

In this section, information pertaining to the dynamical theory of noncentrosymmetric diffraction from a perfect GaAs(111) crystal will be given. The specialization of the analysis for centrosymmetric structures will be straightforward. For a general review of the dynamical theory of x-ray diffraction see Refs. 15 and 16, and for applications of this theory to zinc blende single crystals see Refs. 13 and 8.

For the two-beam plane-wave case of Bragg diffraction from a semi-infinitely thick and symmetrically cut crystal the ratio of the E-field amplitudes can be written[15] as

$$\frac{E_H}{E_0}=-\frac{|P|}{P}\left[\frac{F_H}{F_{\bar{H}}}\right]^{1/2}[\eta\pm(\eta^2-1)^{1/2}]\,, \tag{1}$$

where the dimensionless angular parameter $\eta=\eta'+i\eta''$, with real values η' and η'', is

$$\eta=\frac{-\Delta\theta\sin2\theta_B+\Gamma F_0}{|P|\,\Gamma(F_H F_{\bar{H}})^{1/2}}\,. \tag{2}$$

The structure factor is described in terms of the arrangement of the "N" atoms within the unit cell as

$$F_H=\sum_{n=1}^{N}(f_H^0+f_H'+if_H'')_n e^{2\pi i\vec{H}\cdot\vec{r}_n}\,. \tag{3}$$

The atomic form factor $f_{H,n}^0$ accounts for the coherent scattering of x rays from electrons within the electron distribution of the nth atom. It is energy independent and depends on the magnitude of $\sin\theta/\lambda$. However, if inelastic photon scattering processes are included, the initial and final quantum states affect the phase of a scattered photon. This is usually described by adding a real $f_{H,n}'$ and an imaginary $f_{H,n}''$ anomalous dispersion correction to $f_{H,n}^0$.

Position vector $\vec{r}_n$ locates the center of the nth atom with respect to an arbitrarily chosen reference system. For the case of GaAs we will choose a reference system in which the four Ga atoms in the unit cell have positions (0,0,0) + fcc positions and the four As atoms have positions $(\frac{1}{4},\frac{1}{4},\frac{1}{4})$+fcc positions in a cubic unit cell.

The resulting structure factor $F_H=F_H'+iF_H''$ is complex with real quantities F_H' and F_H'' being

$$F_H'=\begin{cases}4(f_{\mathrm{Ga}}^0+f_{\mathrm{Ga}}'+f_{\mathrm{As}}'')_H & \text{for } h,k,l \text{ all odd and } (h+k+l+1)/4 \text{ an integer}\,,\\ 4(f_{\mathrm{Ga}}^0+f_{\mathrm{Ga}}'-f_{\mathrm{As}}'')_H & \text{for } h,k,l \text{ all odd and } (h+k+l+1)/4 \text{ not an integer}\,,\\ 4(f_{\mathrm{Ga}}^0+f_{\mathrm{Ga}}'+f_{\mathrm{As}}^0+f_{\mathrm{As}}')_H & \text{for } h,k,l \text{ all even and } (|h|+|k|+|l|)/4 \text{ an integer}\,,\\ 4(f_{\mathrm{Ga}}'-f_{\mathrm{As}}'+f_{\mathrm{Ga}}^0-f_{\mathrm{As}}^0)_H & \text{for } h,k,l, \text{ all even and } (|h|+|k|+|l|)/4 \text{ not an integer}\,,\\ 0 \text{ otherwise}\,,\end{cases} \tag{4a}$$

$$F_H''=\begin{cases}-4(f_{\mathrm{As}}^0+f_{\mathrm{As}}'-f_{\mathrm{Ga}}'')_H & \text{for } h,k,l \text{ all odd and } (h+k+l+1)/4 \text{ an integer}\,,\\ 4(f_{\mathrm{As}}^0+f_{\mathrm{As}}'+f_{\mathrm{Ga}}'')_H & \text{for } h,k,l \text{ all odd and} (h+k+l+1)/4 \text{ not an integer}\,,\\ 4(f_{\mathrm{Ga}}''+f_{\mathrm{As}}'')_H & \text{for } h,k,l \text{ all even and } |h|+|k|+|l|)/4 \text{ an integer}\,,\\ 4(f_{\mathrm{Ga}}''-f_{\mathrm{As}}'')_H & \text{for } h,k,l \text{ all even and } (|h|+|k|+|l|)/4 \text{ not an integer}\,,\\ 0 \text{ otherwise}\,.\end{cases} \tag{4b}$$

The "h,k,l all odd" cases of Eq. (4) correspond to noncentrosymmetric planes, which means $F_H\neq F_{\bar{H}}$. The "h,k,l all even with $(|h|+|k|+|l|)/4$ not an integer" case corresponds to a semiforbidden reflection in which the Ga lattice and As lattice do not completely produce destructive interference.

Thermal vibrations are included by multiplying the structure factor with the appropriate Debye-Waller factor e^{-M}. For GaAs(111) we shall approximate the vibrational amplitude of the Ga and As atoms as being equivalent ($e^{-M_{\mathrm{Ga}}}=e^{-M_{\mathrm{As}}}=0.979$, at $T=293$ K).[17]

The reflectivity is $R=|E_H/E_0|^2$. Figure 1 shows calculated GaAs(111) reflectivity curves for x-ray energies close to the Ga ($E_k=10.367$ keV) and As ($E_k=11.863$ keV) K-absorption edges. As can be seen, the shape is strongly influenced by the inelastic absorption process. The E-field intensity at a position $\vec{r}$ in the crystal is proportional to

$$I=e^{-\mu_z z}\left[1+\left|\frac{E_H}{E_0}\right|^2+2P\left|\frac{E_H}{E_0}\right|\cos\left[v-2\pi\frac{\Delta d}{d}\right]\right]\,, \tag{5}$$

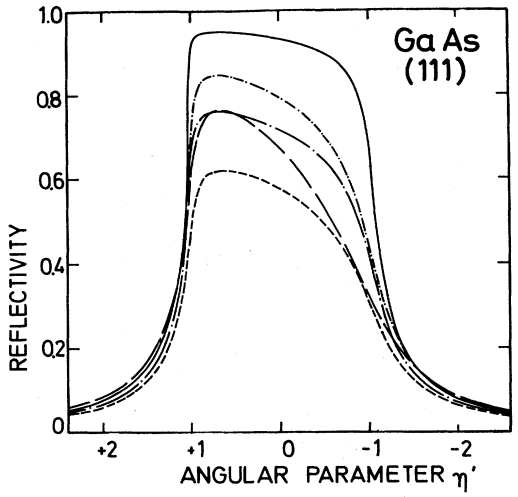

FIG. 1. GaAs(111) theoretical reflection curves at ——, $E_\gamma=10.07$ keV; — — —; $E_\gamma=10.372$ keV; —·—·—·, $E_\gamma=11.16$ keV, ——; $E_\gamma=11.868$ keV, and —·— $E_\gamma=15.1$ keV for the σ polarization state.

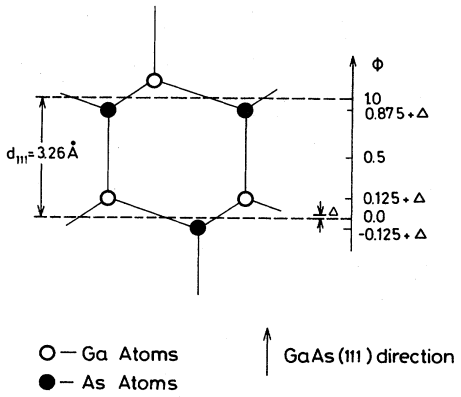

FIG. 2. Schematic view showing the position of the noncentrosymmetric GaAs(111) diffraction planes (dashed lines) relative to the Ga atoms (open circles) and As atoms (closed circles). Parameter Φ locates positions in this structure in the (111) direction relative to a (111) diffraction plane, which is shifted by an amount Δ relative to a centrosymmetric (111) diffraction plane.

where $d=1/|\vec{H}|$ is the d spacing, Δd measures the displacement in the $\vec{H}$ direction from the arbitrarily chosen origin to position $\vec{r}$, and the phase angle

$$v=\tan^{-1}\left[\frac{\mathrm{Im}(E_H/E_0)}{\mathrm{Re}(E_H/E_0)}\right]. \tag{6}$$

The effective linear absorption coefficient μ_z, which is used in Eq. (5), can be expressed as

$$\mu_z=\frac{\mu_0}{\sin\theta_B}\left[1+\frac{P}{F_0''}\mathrm{Im}\left[F_{\bar{H}}\frac{E_H}{E_0}\right]\right], \tag{7}$$

where μ_0 is the normal linear absorption coefficient.

For depths much smaller than the extinction depth, i.e.,

$$z\ll\lambda\sin\theta_B/(2\pi\Gamma)/[\,|F_0''|+(\,|F_H||F_{\bar{H}}|\,)^{1/2}],$$

the exponential attenuation term in Eq. (5) can be neglected. For 15-keV x rays diffracted from GaAs(111) this corresponds to $z\ll 0.3$ μm. Equation (5) indicates that during Bragg diffraction a standing-wave field is produced, which has the same periodicity as the diffraction planes. Furthermore, as the angle of incidence is advanced through the strong Bragg reflection, the phase angle v changes in a linear fashion by π radians, thus causing the antinodes of the standing-wave field to move inward by one half of a d spacing.

In order to find the position of the noncentrosymmetric diffraction planes in this reference system, one applies the condition that the antinodal planes of the E-field intensity coincide positionally with the diffraction planes for $\eta'\le -1$. From Eq. (5), the maximum in the E-field intensity occurs at a position Δd when $\Delta d/d=v/2\pi$. By using $\eta=-1$ in Eq. (1) and the resulting expression in Eq. (6), the diffraction plane position is

$$\frac{\Delta d_0}{d}=\frac{1}{4\pi}\left[\tan^{-1}\left[\frac{F_H''}{F_H'}\right]-\tan^{-1}\left[\frac{F_{\bar{H}}''}{F_{\bar{H}}'}\right]\right]. \tag{8}$$

The expressions in Eq. (4) can be used for describing the centrosymmetric diamond structure case of Ge(111) by replacing both Ga and As with Ge. From this the resulting $\Delta d_0/d=-\frac{1}{8}$. This corresponds to the centrosymmetric diffraction plane position, which is located halfway between the Ga and As layers, as seen in Fig. 2. For the noncentrosymmetric case of GaAs(111), the diffraction planes are shifted from this centrosymmetric position by an amount Δ_{111}. From Eqs. (4) and (8) this noncentrosymmetric shift is

$$\Delta_{111}=-\frac{1}{8}+\frac{1}{4\pi}\left[\tan^{-1}\left[\frac{f^0_{\mathrm{As}}+f'_{\mathrm{As}}+f''_{\mathrm{Ga}}}{f^0_{\mathrm{Ga}}+f'_{\mathrm{Ga}}-f''_{\mathrm{As}}}\right]+\tan^{-1}\left[\frac{f^0_{\mathrm{As}}+f'_{\mathrm{As}}-f''_{\mathrm{Ga}}}{f^0_{\mathrm{Ga}}+f'_{\mathrm{Ga}}+f''_{\mathrm{As}}}\right]\right]. \tag{9}$$

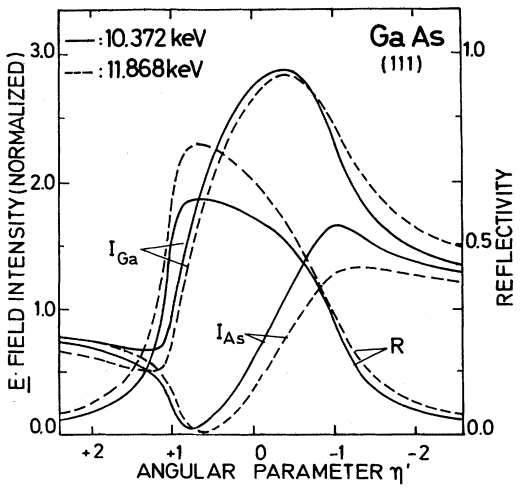

FIG. 3. The angular variation of the GaAs(111) reflectivities (R) and E-field intensities (I_{Ga} and I_{As}) at the Ga and As atomic sites for ——, $E_\gamma=10.372$ keV (5 eV above the Ga K edge), and — — —, $E_\gamma=11.868$ keV (5 eV above the As K edge) (for the σ polarization state).

TABLE I. Calculation of GaAs(111) diffraction plane shift Δ_{111} from atomic scattering factors [see Eq. (9)] using $f^0_{As}=28.170$ and $f^0_{Ga}=26.665$ from Ref. 18, f' and f'' values for 5 eV above the Ga (10.372 keV) and As (11.868 keV) K edges from Ref. 17, and the remaining f' and f'' values from Refs. 19 and 20. The absolute shift in Å can be obtained by multiplying Δ_{111} by $d_{111}=3.26$ Å.

Energy (keV)	f'_{Ga}	f'_{As}	f''_{Ga}	f''_{As}	Δ_{111}
15.1	−0.15	−0.64	2.10	2.59	0.003
11.868	−1.25	−8.0	3.31	5.8	−0.015
11.16	−1.93	−2.82	3.33	0.58	0.001
10.372	−6.0	−2.19	5.0	0.66	0.016
10.07	−3.55	−1.98	0.54	0.70	0.010

Since the dispersion corrections f' and f'' are energy dependent, the position of the diffraction planes with respect to the atomic planes Δ_{111} also depends on the incident x-ray energy.

Hence, for noncentrosymmetric Bragg reflection the diffraction planes have an energy adjustable phase with respect to the atomic lattice. In Fig. 3, the theoretical E-field intensities at the Ga and As atomic sites in GaAs(111) are shown for $E_\gamma=10.372$ keV (5 eV above Ga K edge) and $E_\gamma=11.868$ keV (5 eV above As K edge). At $E_\gamma=10.372$ keV, $\Delta_{111}=0.016$ and at $E_\gamma=11.868$ keV, $\Delta_{111}=-0.015$ (see Table I). Although the resulting shift only corresponds to 0.031 of a d_{111} spacing, the change in the E-field intensity is appreciable as can be seen in Fig. 3. Since the photoelectric absorption of an atom is proportional to the E-field intensity at the site of the atom it becomes possible to determine the energy-dependent position of the diffraction planes by analyzing the yield of the Ga or As photoelectrons during Bragg diffraction.

III. EXPERIMENT

The measurements were carried out with synchrotron radiation generated by the storage ring DORIS at DESY in Hamburg. The instrument ROEMO at the Hamburg Synchrotron Radiation Laboratory provided the basic experimental features for standing-wave measurements.[21] The arrangement is illustrated in Fig. 4. The polarized white spectrum of DORIS gives high angular brightness and photon energies optimized for the absorption edges being studied. A narrow energy band is selected by a double-crystal monochromator using Si(111) single crystals in a parallel mode. The second crystal is asymmetrically cut, having an angle of $\phi=7°$ between the surface and the (111) Bragg planes, thus serving as a plane-wave generator, with a total angular emittance range of 0.67 arc sec at 15.1 keV. This width is small compared to that of the GaAs(111) reflection from the sample (8.3 arc sec). Since the respective (111) d spacings for the Si, GaAs, and Ge lattice planes differ only slightly, the dispersion of the arrangement is normally small enough for standing-wave applications. Ge(111) data, which we have measured, are not discussed in detail to limit the total length of this paper.

The sample is built into a gas flow proportional detector.[22,23] Photoelectrons and Auger electrons, emitted from the sample, ionize the gas volume, which consists of a 90% helium + 10% methane mixture. After gas multiplication, the resulting cascade is collected at a 20-μm-thin gold wire. The efficiency of the chosen gas mixture is very high for ionization by electrons with a kinetic en-

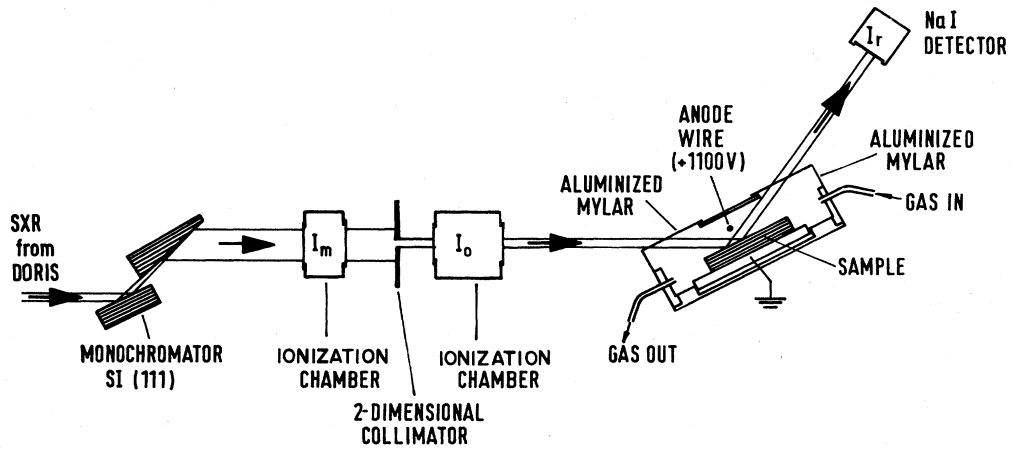

FIG. 4. Experimental setup (schematic side view).

ergy in the keV range and very small ($\lesssim 1\%$) for the incident and reflected synchrotron X radiation. With a multichannel analyzer operated in a multispectrum scaling mode up to 32 subgroups are collected with different electron yield spectra. Each subgroup is directly related to a small angular fraction of the sample reflection curve.[21] The resolution of the detector is about 1 keV for the electron energies used. The whole detector was mounted on an Eulerian cradle with a special stage for standing-wave experiments.[24] The reflected intensity was monitored with a NaI(Tl) detector. In this experimental arrangement, the horizontal polarization direction of the synchrotron radiation is perpendicular to both the incident and diffracted wave vectors. This corresponds to the σ polarization state.

The total electron yield from the sample was approximately 5×10^{-4} electrons per photon, at an incident photon energy of 15 keV. Since the primary beam contains about 10^8 phot/mm^2, small sample areas are sufficient to provide enough signal to perform standing-wave analysis. Therefore, with a two-dimensional collimator, the proper region of the crystal can be chosen and three-dimensional information can be extracted about crystal defects, epitaxially grown layers or amorphous surface layers.[25] Planar information is obtained by scanning and the depth profile is connected with the electron energy-loss process as described in the following sections.

IV. ELECTRON YIELD SPECTRA

Electrons only have a very short mean-free path before they undergo an inelastic electron-electron or electron-plasmon interaction. Therefore, they reach the surface with an energy loss, which depends upon their origin and upon the sample material. When they originate from layers close to the surface, this loss can be zero.

Electron yield spectra which were recorded with the previously described detector are shown in Fig. 5. Also shown is an absorption spectrum which was measured by using the total electron yield signal being proportional to the number of photons absorbed in the sample.

Curve 5(a) at the bottom was measured for a photon energy just below the Ga K-absorption edge. The broad photoelectron peak mainly consists of L photoelectrons which have a maximum energy of $E_{\mathrm{kin,max}}=E_\gamma-E_{L_3}=8.95$ keV, where E_γ and E_{L_3} correspond to the photon energy and to the L_3 Ga binding energy, respectively. Also contributing are electrons from other Ga L subshells as well as from As L states. The yield at energies closer to E_γ is affected by transitions from outer M and valence states. However, the cross section for photoabsorption of these outer electrons is much smaller. This can be seen for the respective cross sections[26] of Ga. At 9.88 keV (Ge $K\alpha$ line) $\sigma_L=3190$ b/atom, $\sigma_M=471$ b/atom, and $\sigma_N=15.2$ b/atom.

At an energy 5 eV above the Ga K absorption edge [Fig. 5(b)], K-photoelectron emission as well as KXY Auger electron emission are turned on. For the case of KL_2L_3 these Auger electrons are clearly visible in the increased yield below the energy $E_{\mathrm{kin,Auger}}=8.04$ keV. K photoelectrons are not detected because their kinetic energy is too small ($\lesssim 5$ eV).

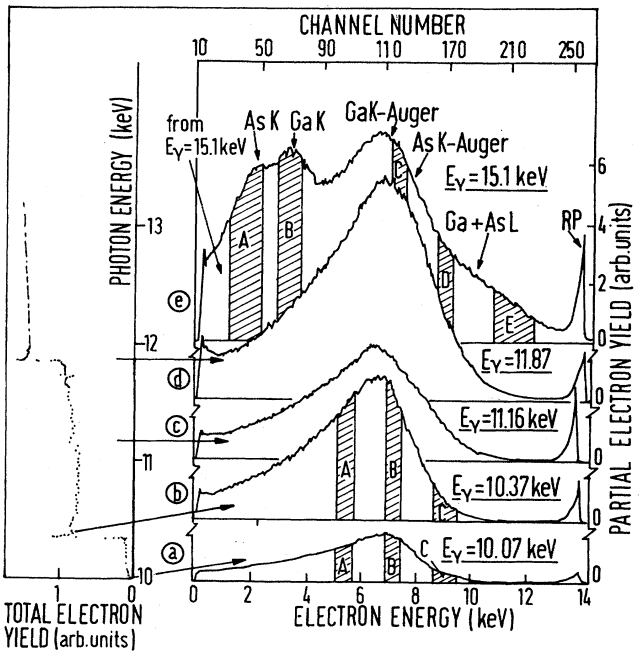

FIG. 5. Off Bragg GaAs electron yield spectra collected with a gas flow proportional detector at incident x-ray energies in the vicinity of the respective K absorption edges of Ga and As. Owing to the E_γ-dependent stopping power of the I_0 ionization chamber, the partial yield curves (a)—(e) were multiplied by 0.86, 0.91, 1.0, 1.1, and 2.0, respectively. The absorption spectrum that was obtained while calibrating the incident x-ray energy scale for this set of experiments is shown as a side view on the left. RP represents the reference pulser.

As one increases the energy to above the As K-absorption edge, KXY Auger electrons from As atoms are emitted [Fig. 5(d)]. The Ga K photoelectrons now have enough kinetic energy so that they appear in the peak at

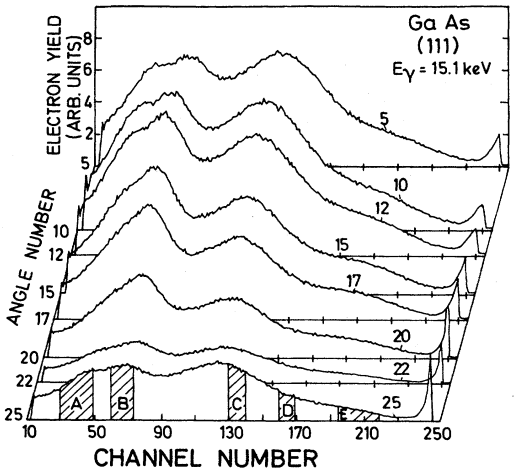

FIG. 6. Electron yield spectra collected at different angular positions of the rocking curve, while Bragg diffracting from a GaAs(111) single crystal with a 15.1-keV incident x-ray beam. The corresponding rocking curve, shown in Fig. 7, illustrates the angular scale.

about 500 eV. When the energy is raised further to 15.1 keV [Fig. 5(e)], both Ga and As K photoelectron peaks are clearly distinguishable.

The energy scale which is given for these spectra has been determined by comparing the same electron process at different photon energies. The Auger electron yield for example can be extracted by subtracting the spectrum below an absorption edge from that above the edge.

As described in Sec. II, the standing-wave pattern created inside the sample crystal under the condition of Bragg reflection can be moved across the netplanes by changing the reflection angle. Electron yield spectra which were measured with a fixed photon energy at several angles within and just outside the total reflection range are shown in Fig. 6. Note, that the As K-photoelectron peak (region A) is strongly depressed at angle position 20. Referring to Fig. 2 this corresponds to a node in the wave field being located at $\Phi=-0.125+\Delta$, right on the As atom sites. At angle position 10, the high-angle side of the reflection range (Fig. 7), the maxima of the standing-wave pattern lie on the diffraction planes $\Phi=0$. This behavior demonstrates the possibility of determining the polarity of the crystal by one single measurement. Reflecting at $(\bar{1}\bar{1}\bar{1})$ planes exchanges the Ga and As atomic planes in Fig. 2.

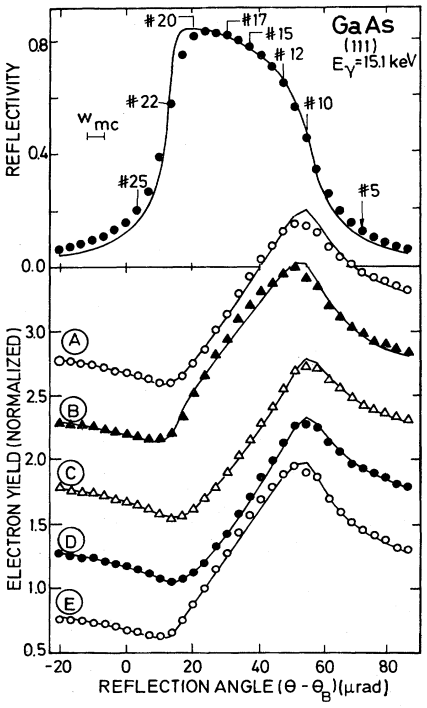

FIG. 7. Reflection data and theory for Bragg diffraction from the GaAs(111) sample at $E_\gamma=15.1$ keV and the corresponding angular variation to the electron yields of electron energy regions A, B, C, D, and E [see Fig. 5(e)]. The electron yield scale corresponds to the bottom curve. Subsequent curves are given 0.5, 1.0, 1.5, etc., offsets, respectively.

V. DATA ANALYSIS AND RESULTS

A primary objective of an x-ray-standing-wave analysis is to determine the atomic distribution function of a particular set of atoms. This is usually characterized by the coherent fraction f_c of atoms occupying coherent positions Φ_c in units of the diffraction plane spacing d_{hkl}. When using a detector system with sufficient energy resolution it is possible to identify Φ_c and f_c with a specific set of atoms (Ga or As) undergoing selective excitation of a particular electron state. For the $\sim$1-keV resolution of our electron counter and a sample with two almost adjacent elements, the measured electron yield contains in each electron energy region of the spectrum, contributions from both Ga and As. However, f_c and Φ_c still contain useful structural information which will be demonstrated in this analysis by combining measurements at different photon energies.

The coherent position and fraction for a particular electron energy region is determined by fitting the experimental angular yield for this region to angular E-field intensity expressions based on dynamical diffraction theory. For the experimental angular yield, the total counts in each region were normalized for dead-time effects and then given a pulse pileup correction. The lifetime for each spectrum was determined from the random reference pulser signal. The pulse pileup correction was determined by an experimental simulation.

The theoretical model that was given a χ^2 fit to the experimental angular yield data has the form

$$Y(\theta,\Phi_c,f_c,z)=f_c I(\theta,\Phi_c,z) + (1-f_c)[1+R(\theta)]e^{-\mu_z z}. \quad (10)$$

The E-field intensity $I(\theta,\Phi_c,z)$ is given in Eq. (5), R is the reflectivity, μ_z is the effective absorption coefficient described by Eq. (7). The first term in Eq. (10) corresponds to the angular yield from a coherent fraction f_c of atoms, which have the periodicity of the diffraction planes and are at a coherent position Φ_c with respect to the diffraction planes (see Fig. 2 for an explanation of the Φ scale). The second term describes the remaining fraction of atoms as being randomly distributed. The $e^{-\mu_z z}$ factor in both terms accounts for the angular-dependent attenuation of the x-ray wave field (extinction effect). In our analysis we approximate that all of the electrons in a given electron energy region originate from the same depth z. This depth z was not a variable parameter for the GaAs(111) data analysis, but was predetermined from Ge(111) data. This was a necessary procedure since the parameters z and Φ_c do not correlate well in the fitting process. For the Ge(111) data analysis the coherent position was naturally fixed at $\Phi_c=0$. Inclusion of the $e^{-\mu_z z}$ attenuation factor significantly improved the least-square fits of Eq. (10) to the experimental angular yield data.

Although the detailed electron scattering process causes a complicated depth profile for electrons escaping from the solid with a particular energy loss, the above single-depth approximation for this profile is sufficient for the analysis, provided that the electron escape depth is smaller than the x-ray extinction depth.

The validity of modeling the distribution of atoms as a

coherent fraction f_c at a position Φ_c and the remaining fraction of atoms being randomly distributed stems from the fact that the x-ray-standing-wave measurement determines the (hkl) Fourier component of the distribution function of inelastic scatterers.

For a particular electron energy region the distribution function of Ga and As atoms with a (111) d-spacing periodicity can be written as

$$g(\Phi)=G\delta(\Phi-\tfrac{1}{8}-\Delta)+(1-G)\delta(\Phi+\tfrac{1}{8}-\Delta)\ , \qquad (11)$$

where G represents the fractional yield of the electron energy region which originated from Ga atoms at position $\Phi=\frac{1}{8}+\Delta$ (see Fig. 2). Likewise $(1-G)$ represents the As contribution from $\Phi=-\frac{1}{8}+\Delta$. The (111) Fourier coefficient of this distribution function is

$$F_1=G\,e^{2\pi i(1/8+\Delta)}+(1-G)e^{2\pi i(-1/8+\Delta)}\ . \qquad (12)$$

With $F_1=|F_1|e^{2\pi i\Phi_1}$, the amplitude of the Fourier coefficient, which is directly related to the coherent fraction f_c, is

$$|F_1|=(2G^2-2G+1)^{1/2}\ , \qquad (13)$$

and the phase of the Fourier coefficient, which is directly related to the coherent position Φ_c, is

$$\Phi_1=\frac{1}{2\pi}\tan^{-1}\left[\frac{2G-1+\tan(2\pi\Delta)}{(1-2G)\tan(2\pi\Delta)+1}\right]\ . \qquad (14)$$

The above distribution function $g(\Phi)$ assumes that the atoms are fixed points relative to the diffraction planes. To include thermal vibrations, the δ functions of Eq. (11) are replaced with normalized Gaussian functions[23] having widths $\sigma=(\langle u^2\rangle)^{1/2}/d$, where $(\langle u^2\rangle)^{1/2}$ is the root mean square of the vibrational amplitude. We will use $(\langle u^2\rangle)^{1/2}=0.107$ Å for both Ga and As at room temperature. (Note that $e^{-2\pi^2\sigma^2}=e^{-M}=0.979$.) The consideration of thermal vibrations adds a prefactor to Eq. (13) yielding

$$|F_1|=e^{-M}(2G^2-2G+1)^{1/2}\ . \qquad (15)$$

In examining the expressions given in Eqs. (14) and (15), it is evident that for an electron energy region with no contribution from As sites (i.e., $G=1$), $|F_1|=e^{-M}=0.979$ and $\Phi_1=\frac{1}{8}+\Delta$. The smallest Fourier amplitude is produced for an equal contribution from the Ga and As sites (i.e., $G=\frac{1}{2}$). In this case $|F_1|=e^{-M}/\sqrt{2}=0.692$ and $\Phi_1=\Delta$. For the Ge(111) case, it is not possible to spectroscopically discriminate between the $\Phi=\frac{1}{8}$ and $-\frac{1}{8}$ positions; therefore, the coherent fraction and position for Ge(111) should ideally be $f_c=e^{-M}/\sqrt{2}$ and $\Phi_c=0$ for all electron energy regions.

The experimental electron yields versus angle for the electron energy regions designated in Figs. 5(e), 5(b), and 5(a) are shown in Figs. 7, 8, and 9, respectively. The χ^2 fitted curves are based on Eq. (10). The determined values for f_c and Φ_c and the fixed z values are shown in Table II for the $E_\gamma=15.1$ keV and 10.07 keV GaAs(111) data sets. As previously stated, the average electron escape depth values z were determined from the corresponding Ge(111) data sets.

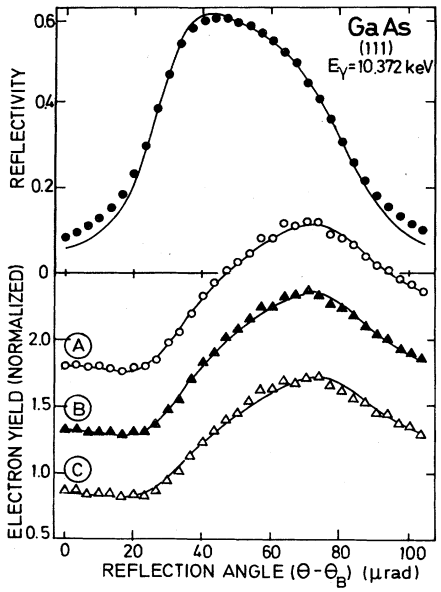

FIG. 8. Same as Fig. 7, but for $E_\gamma=10.372$ keV [see Fig. 5(b)].

The experimental reflection curve for each of these x-ray-standing-wave scans is also shown in Figs. 7, 8, and 9. The fitted theoretical reflectivity curves were used to determine the angular scale for each scan. The angular range from each of the three fits was 103 ± 2 μrad. The theoretical reflectivity and E-field intensities for the 15.1-keV scan were not convoluted with the angular output from the asymmetrically cut ($\phi=7°$) Si(111) monochromator crystal, since the ratio of this width (ω_{mc}) to the GaAs(111) acceptance width was $\frac{1}{12}$. However, since this ratio was approximately $\frac{1}{4}$ for the x-ray-standing-

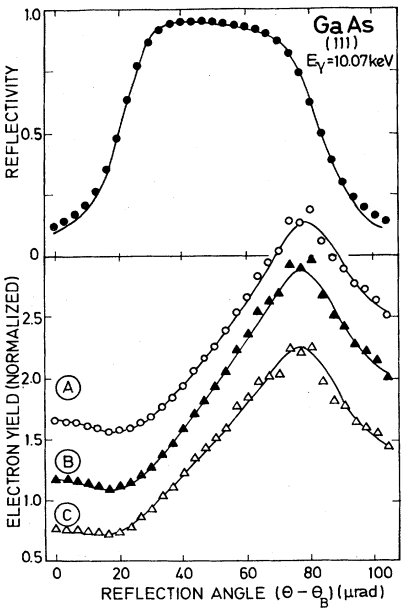

FIG. 9. Same as Fig. 7, but for $E_\gamma=10.07$ keV [see Fig. 5(a)].

TABLE II. Data analysis [see Figs. 5(a), 5(e), 7, and 9].

E_γ (keV)	Electron-energy region	Average electron escape depth z (Å)	Coherent fraction f_c (± 0.01)	Coherent position Φ_c (± 0.004)	Ideal coherent $\lvert F_1 \rvert$	GaAs(111) $\frac{f_c}{\lvert F_1 \rvert}$	Ge(111) $\frac{f_c}{\lvert F_1 \rvert}$
15.1	*A*	920	0.69	−0.022	0.70	0.92	0.97
15.1	*B*	1060	0.64	+0.036	0.71	0.90	0.95
15.1	*C*	1430	0.67	−0.035	0.71	0.94	0.97
15.1	*D*	1150	0.67	−0.040	0.72	0.94	0.97
15.1	*E*	880	0.63	+0.002	0.69	0.91	0.95
10.07	*A*	1170	0.70	−0.012	0.70	0.99	0.95[a]
10.07	*B*	700	0.68	−0.010	0.70	0.97	0.94[a]
10.07	*C*	650	0.55	−0.008	0.70	0.79	0.87[a]

[a]Ge(111) data at $E_\gamma = 10.9$ keV.

wave scans at 10.372 and 10.07 keV, the theoretical GaAs(111) reflectivity and intensity curves were convoluted by the angular output from the monochromator.

Since the experimental angular scan range for each of the separate x-ray energies was maintained at a constant setting ($\pm 1\%$), it was possible to confirm the f' values in Table I to within 10% by noting that the theoretically fit determined range of 103 ± 2 μrad was maintained for each of the five energies and by assuming the values at 15.1 keV. If wanted, this precision can easily be increased.

VI. DISCUSSION

From the average electron escape depth values listed in Table II it can be seen that as the electron energy loss for a particular electron-emission process increases, the depth z also increases. Furthermore, these depth values fall in line with empirically calculated values [7] for the emergence length of electrons emitted in Ge; $L_e = 250 E_i^{1.4}$ Å, where E_i is the initial kinetic energy of the escaping electron in keV. For Ge L photoelectrons ejected by photons having energy $E_\gamma = 10$ keV, $L_e = 5200$ Å. The energy resolution of the electron counter was insufficient to spectroscopically separate the electrons emitted from the Ga and As atomic sites. Therefore, the measured coherent position values Φ_c in Table II do not reach the pure Ga value of $0.125 + \Delta$ or the pure As value of $-0.125 + \Delta$. The data taken just above the Ga K-absorption edge [Figs. 5(b) and 8] most closely approach this one site condition since the Ga KLL Auger electron yield is anomalously very high at this energy.

The most straightforward way of testing this data analysis for an x-ray energy-dependent diffraction plane shift is to look for a shift in the measured coherent position Φ_c for electron energy regions that have the same distribution of inelastic scattering sources at two different x-ray energies.

For this comparison we will choose the highest electron energy region in the $E_\gamma = 15.1$ keV scan and any of the electron energy regions in the $E_\gamma = 10.07$ keV scan. These regions have comparable Ga contributions G, since each has no K photoelectrons nor any K Auger electrons. Based on the non-K-photoelectric cross sections[26] the Ga contribution in all four of these electron energy regions should be $G = 0.43$. From Eq. (14) it can be seen, that for constant G, a shift in the coherent position Φ_c is directly attributable to a shift in the diffraction plane position Δ_{111}. Since the coherent position for the three regions of the $E_\gamma = 10.07$ keV scan is $\Phi_c = -0.010 \pm 0.006$ and since $\Phi_c = 0.002 \pm 0.004$ for region E of the 15.1 keV scan, it can be seen that there is an energy-dependent diffraction plane shift of 0.012 ± 0.007. From the atomic scattering factors given in Table I this shift was calculated as being 0.007 and agrees within the error limits.

We have also included in Table II the result for the ideal coherent fraction $\lvert F_1 \rvert$ which is calculated from Eqs. (14) and (15) by using the measured coherent position Φ_c along with the Δ_{111} values listed in Table I. The comparison ratio $f_c / \lvert F_1 \rvert$ shows a deviation from unity which can be caused by three different effects: (i) Owing to experimental angular averaging $f_c / \lvert F_1 \rvert$ never reaches unity for any of the electron energy regions. (ii) The presence of disordered bulk or disordered surface layers can reduce the coherent fraction for electrons with a specific energy loss.[25] (iii) The different spatial distinctions of the K, L, M, and N electrons will influence the coherent fractions of electrons emitted from different orbitals. This will be visible in sudden variations of f_c at certain electron energies. Although such changes clearly show up in Table II, a detector with higher energy resolution is needed to separate out these effects distinctively.

VII. CONCLUSION

We have demonstrated that x-ray-standing-wave—modulated electron emission measurements, with a low-resolution electron counter, can be used to obtain valuable information about a crystal structure, such as the polarity, the degree of perfection, and the position of the constituent atoms. With the high intensity of synchrotron radiation, it is possible to study very small crystal areas and by making use of the depth-dependent energy-loss process for electron emission, depth-selective structural

information is also obtainable. The tunability of the photon energy, which is provided by a synchrotron source, can be successfully applied to measure electron yields and reflectivity curves in the vicinity of absorption edges. Thus making it possible to determine the anomalous dispersion parameters f' and f'', which describe the energy dependence of the x-ray scattering process. By using the x-ray-standing-wave picture for describing the dynamical scattering process in a zinc blende single crystal, the energy dependence of the position of the noncentrosymmetric diffraction planes was also demonstrated. Since this measuring technique makes it possible to separate the x-ray scattering process into its various contributing channels, further explorations should be made in this direction with a medium or high-energy resolution electron detector.

[1]G. Borrmann, Z. Phys. A **2**, 157 (1941); **127**, 297 (1950).
[2]B. W. Batterman, Phys. Rev. **133**, A759 (1964).
[3]S. Annaka, S. Kikuta, and K. Kohra, J. Phys. Soc. Jpn. **21**, 1559 (1966).
[4]A. M. Afanasev and S. L. Azizian, Acta. Crystallogr. A **37**, 125 (1981).
[5]J. A. Golovchenko, D. R. Kaplan, B. Kincaid, R. Levesque, A. Meixner, M. F. Robbins, and T. Felsteiner, Phys. Rev. Lett. **46**, 1454 (1981).
[6]W. Schülke, Phys. Lett **83A**, 451 (1981).
[7]M. V. Kruglov, E. A. Sozontov, V. N. Shchemelev, and B. G. Zakharov, Kristallografiya **22**, 693 (1977) [Sov. Phys. Crystallogr. **22**, 397 (1977)], and references therein.
[8]T. Takahashi and S. Kikuta, J. Phys. Soc. Jpn. **47**, 620 (1979).
[9]J. A. Golovchenko, B. W. Batterman, and W. L. Brown, Phys. Rev. B **10**, 4239 (1974).
[10]P. L. Cowan, J. A. Golovchenko, and M. F. Robbins, Phys. Rev. Lett. **44**, 1680 (1980).
[11]J. A. Golovchenko, J. R. Patel, D. R. Kaplan, P. L. Cowan, and M. J. Bedzyk, Phys. Rev. Lett. **49**, 560 (1982).
[12]V. G. Kohn, M. V. Kovalchuk, R. M. Imamov, B. G. Zakharov, and E. F. Lobanovich, Phys. Status Solidi A **71**, 603 (1982).
[13]P. Trucano, Phys. Rev. B **13**, 2524 (1976).
[14]J. R. Patel and J. A. Golovchenko, Phys. Rev. Lett. **50**, 1858 (1983).
[15]B. W. Batterman and H. Cole, Rev. Mod. Phys. **36**, 681 (1964).
[16]Z. G. Pinsker, *Dynamical Scattering of X-Rays in Crystals* (Springer, Berlin, 1978).
[17]T. Fukamachi, S. Hosoya, T. Kawamura, and M. Okunuki, Acta. Crystallogr. A **35**, 828 (1979).
[18]J. H. Hubbell and I. Øverbø, J. Phys. Chem. Ref. Data **8**, 69 (1979).
[19]*International Tables for X-Ray Crystallography* (Kynoch, Birmingham, England, 1962), Vol. III.
[20]L. Gerward, Nucl. Instrum. Methods **181** 11 (1981).
[21]G. Materlik and J. Zegenhagen (unpublished).
[22]N. Hertel, M. V. Kovalchuk, A. M. Afanesev, and R. M. Imamov, Phys. Lett. **75A**, 501 (1980).
[23]N. Hertel, thesis, University of Aarhus, 1981.
[24]A. Krolzig, G. Materlik, and J. Zegenhagen, Nucl. Instrum. Methods **208**, 613 (1983).
[25]M. Bedzyk, G. Materlik, and M. V. Kovalchuk (unpublished).
[26]G. Hildebrand, J. D. Stephenson, and H. Wagenfeld, Z. Naturforsch. **30A**, 697 (1975).